International Journal of Advanced Trends in Computer Applications
*www.ijatca.com*

# Analysis of stability and dual solution of MHD outer fluid velocity with partial slip on a stretching cylinder

**[1]Vikas Poply, [2]Phool Singh, [3]A. K. Yadav**
[1]Department of Mathematics, KLP College, Rewari, India
[2]Department of Applied Sciences, Central University Haryana, India
[3]Department of Applied Mathematics, ASAS, Amity University, Gurgaon, India
*[1]vikaspoply@yahoo.com, [2]phoolsingh@cuh.ac.in, [3]aky68@yahoo.com*

**Abstract:** *This manuscript discuss about the dual nature of solution, in MHD outer velocity flow, along with the stability analysis on stretching cylinder with partial slip. Differential equations are acquired by converting heat and momentum governing equations with similarity transformations. The numerical solutions of the transformed equations were computed by the Runge-Kutta Fehlberg scheme using shooting procedure. For stretching cylindrical surface, we obtained that the solution is not unique having partial slip. The dual nature of the solution exists in small range of outer velocity parameter on stretching surface. Stability analysis reveals that for lower branch (unstable solution) and upper branch (stable solution), the smallest eigenvalue is negative and positive respectively for the distinct entries of outer velocity parameter. The limit of the dual solution is -0.03211 =* $\boldsymbol{\lambda_c \leq \lambda \leq \lambda_r}$ *= 0.12651 for slip parameter,* $\boldsymbol{V = 0.1}$. *Also, the influences of slip parameter, outer velocity parameter and magnetic parameter have been discussed on heat and flow transportation, which are presented through tables and figures.*

**Keywords:** Partial slip, Stretching cylinder, MHD, Stability analysis.

## I. INTRODUCTION

Numerous practical applications of heat and flow transportation in several divisions of manufacturing procedure lead attention of many researchers in this field of stretching surface. During these processes, sometimes the strips are stretched thereby affecting the final product. Therefore, for researchers, study of heat and flow transportation has acquired much consideration over stretching surfaces because of their industrial applications in polymer extrusion, wire drawing and paper production etc. The impact of flow behavior over a stretched sheet was initiated by Crane (1970). Due to wide-ranging applications of stretching material in manufacturing processes, researchers got interested in investigating the rate of transference of heat over stretching surfaces (Gupta and Gupta, 1977; Ali, 1994; Singh et al., 2010) as an extension of Crane (1970) in the field of heat transfer. There are many physical/industrial phenomenons in which the boundary surface closely resembles cylindrical geometry. In such processes, the impacts of heat and flow transportation over cylindrical stretched surfaces are essential. These processes comprise of wire drawing, hot rolling, and spinning of fibers etc.

The applications of stretching surfaces in industries includes polymer extrusion process, paper production etc. Therefore, the flow characteristics over static and stretching cylinder have been initiated by Lin and Shih (1980) and Wang (1988) respectively. Magnetic field plays a significant role in many industrial applications like petroleum refining, power generation, and cooling of objects etc. The MHD effect over a stretching cylinder has been studied by Ishak et al. (2008) and its few extensions have been reported in (Vajravelu et al., 2012; Yadav and Sharma, 2014; Malik et al., 2015) with different physical conditions. These studies have confirmed that fluid velocity is strongly influenced by magnetism. In some manufacturing processes, which involve process of filtration and controlling of heat generation, the effect of outer flow becomes significant. The effect of free stream flow on heat and mass transportation over vertical and horizontal cylinder has been studied by Takhar et al. (2000) and

Lok et al. (2012) respectively. None of the studies cited above has reported the existence of dual solution and carried out stability analysis. The stability analysis flow solution about stagnation-point over stretching surfaces has been discussed in detail in (Paullet and Weidman, 2007; Mahapatra et al., 2012; Sharma et al., 2014; Dhanai et al., 2015; Awaludin et al., 2016). Poply et al. (2018) reported that the dual solution exist for stretching cylindrical surfaces.

In all of the above studies mentioned so far, the partial slip flow has not been considered. Partial slip occur when the fluid contains particulates; for example, suspensions, emulsions, polymer solutions and foams. The partial slip fluids are important in manufacturing processes, like spinning motion and filtration process. Therefore, the effect of slip velocity on stretching surfaces has been discussed by (Andersson, 2002; Ariel, 2008). The effect of slip flow on stretching cylinder in quiescent fluid has been examined in (Wang and Ng, 2011; Mukhopadhyay, 2013; Mat et al., 2015) and they reported that velocity of the fluid reduces in presence of slip surface. Critical values in slip flow in a non-Newtonian nanofluid have been reported by Dhanai et al. (2016).

The above literature survey reveals that no study had discussed so far, for stretching cylindrical surface, for calculating the flow stability in outer fluid MHD flow with partial slip. In current analysis, we investigate the same effect and results of this investigation explains that the smallest eigenvalue approaches to zero for both unstable and stable solution as the outer velocity parameter approaches to the critical point of outer velocity parameter.

## II. PROBLEM FORMULATION

We have considered a electrical conducting, partial slip, axisymmetric steady flow of a non-compressible fluid over stretching cylinder having constant radius a (Figure 1). The magnetic field applied radially with intensity $B_o$. Due to the applied magnetic field, the magnetic field which is induced being very small and that can be neglected. The stretching surface temperature $T_w(x)$ and velocity $u_w(x)$ are prescribed according to the following expressions:

$$T_w(x) = T_\infty + T_0\left(\frac{x}{l}\right)^n \quad \text{and} \quad u_w(x) = c\left(\frac{x}{l}\right).$$

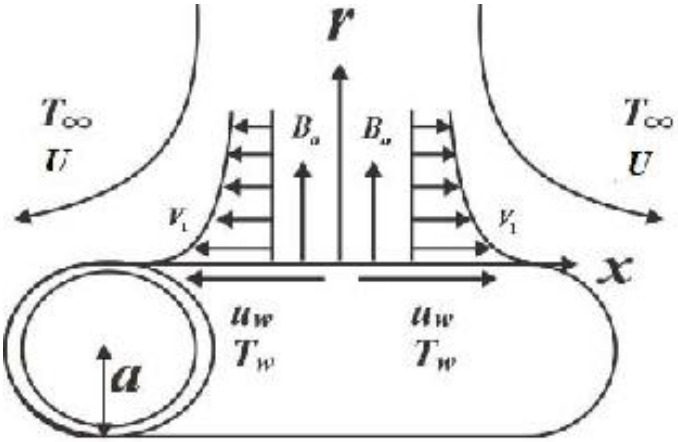


**Figure 1:** Schematic diagram

Here, $n$ be exponent of temperature. The governing equations of above considered problem are described as:

$$\frac{\partial(ru)}{\partial x} + \frac{\partial(ru)}{\partial r} = 0 \tag{1}$$

$$u\frac{\partial u}{\partial x} + v\frac{\partial u}{\partial r} = U\frac{\partial U}{\partial x} + \frac{\nu}{r}\frac{\partial}{\partial r}\left(r\frac{\partial u}{\partial r}\right) - \frac{\sigma B_0^2}{\rho}(u - U) \tag{2}$$

$$u\frac{\partial T}{\partial x} + v\frac{\partial T}{\partial r} = \frac{\alpha}{r}\frac{\partial}{\partial r}\left(r\frac{\partial T}{\partial r}\right) \tag{3}$$

where velocity along $r$ and $x$- axes are taken as $v$ and $u$ respectively.$\nu, B_{0,} \rho, \sigma,$ U, T and $\alpha$ be the kinematic viscosity, magnetic field strength, density, electrical conductivity, outer velocity, temperature and thermal diffusivity respectively.

The relevant restrictions on boundary are:

$$\begin{cases} At\ r = a, T = T_w(x), u = u_w(x) + V_o v\dfrac{\partial u}{\partial r}\ \ and\ \ v = 0 \\ \qquad As\ r \to \infty, T \to T_\infty\ and\ u \to U = b\left(\dfrac{x}{l}\right) \end{cases} \tag{4}$$

Here, $V_o$ represents slip velocity.

Writing $v$ and $u$ in terms of $\psi(x,r)$ (stream function) as $v = -\frac{1}{r}\frac{\partial \psi}{\partial x}\ and\ u = \frac{1}{r}\frac{\partial \psi}{\partial r}$ the continuity equation (1) is satisfied.

Introducing similarity variables
$\eta = \frac{r^2-a^2}{2a}\sqrt{\frac{u_w}{vx}}, \psi = \sqrt{u_w\, vx}af(\eta)\ and\ \theta = \frac{T-T_\infty}{T_w-T_\infty}$ (dimensionless temperature), the equation (2) and (3) are transformed as

$$(1+2\gamma\eta)f''' + 2\gamma f'' + ff'' - f'^2 - M(f' - \lambda) + \lambda^2 = 0 \tag{5}$$
$$(1+2\gamma\eta)\theta'' + 2\gamma\theta' + \Pr(f\theta' - nf'\theta) = 0 \tag{6}$$

The transformed conditions on the boundary are:

$$\begin{cases} \theta(0) = 1, f'(0) = 1 + Vf''(0), f(0) = 0 \\ \qquad \theta(\infty) = 0, f'(\infty) = \lambda \end{cases} \tag{7}$$

where $\gamma = \frac{1}{a}\sqrt{\left(\frac{vl}{c}\right)}$, $V = V_o\sqrt{\frac{cv}{l}}$, $Pr = \frac{v}{\alpha}$, $\lambda = \frac{b}{c}\ and\ M = \frac{\sigma B_0^2 l}{\rho c}$ represents the curvature parameter, slip parameter, Prandtl number, outer velocity parameter and magnetic parameter respectively.
The Nusselt number $N_u$ and coefficient of skin friction $C_f$ are described as

$$N_u = -\sqrt{Re}\bar{x}\theta'(0)\ and\ C_f = \frac{2\bar{x}f''(0)}{\sqrt{Re}}$$

where $Re(= lc/v)$ represents the Reynolds number.

## III. STABILITY ANALYSIS

Unsteady case is considered for analyzing the flow stability and equations (2) and (3) are rewritten as:

$$\frac{\partial u}{\partial t} + u\frac{\partial u}{\partial x} + v\frac{\partial u}{\partial r} = U\frac{\partial U}{\partial x} + \frac{v}{r}\frac{\partial}{\partial r}\left(r\frac{\partial u}{\partial r}\right) - \frac{\sigma B_0^2}{\rho}(u - U) \tag{8}$$

$$\frac{\partial T}{\partial t} + u\frac{\partial T}{\partial x} + v\frac{\partial T}{\partial r} = \frac{\alpha}{r}\frac{\partial}{\partial r}\left(r\frac{\partial T}{\partial r}\right) \tag{9}$$

For solving the above system of equations, we add $\tau(= (\frac{c}{l})t)$ along with $\eta, \psi\ and\ \theta$ as a similarity variable. By applying similarity variables, the equations (8) and (9) are reduced to

$$(1+2\gamma\eta)\frac{\partial^3 f}{\partial \eta^3} + 2\gamma\frac{\partial^2 f}{\partial \eta^2} + f\frac{\partial^2 f}{\partial \eta^2} - \left(\frac{\partial f}{\partial \eta}\right)^2 - M\left(\frac{\partial f}{\partial \eta} - \lambda\right) + \lambda^2 - \frac{\partial^2 f}{\partial \eta \partial \tau} = 0 \tag{10}$$

$$(1+2\gamma\eta)\frac{\partial^2 \theta}{\partial \eta^2} + 2\gamma\frac{\partial \theta}{\partial \eta} + Pr\left(f\frac{\partial \theta}{\partial \eta} - n\frac{\partial f}{\partial \eta}\theta\right) - \frac{\partial \theta}{\partial \tau} = 0 \tag{11}$$

and corresponding boundary restrictions become

$$\theta(0,\tau) = 1, f(0,\tau) = 0, \frac{\partial f}{\partial \eta}(0,\tau) = 1 + V\frac{\partial^2 f}{\partial \eta^2}(0,\tau),$$

$$\theta(\infty,\tau) = 0, \frac{\partial f}{\partial \eta}(\infty,\tau) = \lambda \tag{12}$$

We consider, $f(\eta) = f_0(\eta)$ and $\theta(\eta) = \theta_0(\eta)$ as a solution of equations (1)-(4), and follow the method of Merkin (1985) by adopting

$$f(\eta,\tau) = f_0(\eta) + e^{-s\tau}F(\eta,\tau) \text{ and } \theta(\eta,\tau) = \theta_0(\eta) + e^{-s\tau}G(\eta,\tau) \tag{13}$$

where $s$ represents eigenvalue, and $F(\eta,\tau)$ and $G(\eta,\tau)$ are assumed to be insignificant in respect of $f_0(\eta)$ and $\theta_0(\eta)$. Solutions of problem (10)-(12) gives an unbounded eigenvalues as $s_1 < s_2 < \ldots$ The negative and positive smallest eigenvalue indicates an initial growth and decay in the disturbance respectively and thus the flow is unstable and stable accordingly.

Substituting equation (13) in equations (10)-(12), we get

$$(1+2\gamma\eta)\frac{\partial^3 F}{\partial\eta^3}+(2\gamma+f_0)\frac{\partial^2 F}{\partial\eta^2}+f_0^{''}F-(2f_0^{'}-s+M)\left(\frac{\partial F}{\partial\eta}\right)-\frac{\partial^2 F}{\partial\eta\partial\tau}=0 \quad (14)$$

$$(1+2\gamma\eta)\frac{\partial^2 G}{\partial\eta^2}+2\gamma\frac{\partial G}{\partial\eta}+Pr\left[f_0\frac{\partial G}{\partial\eta}+\theta_0^{'}F-n\left(f_0^{'}G+\theta_0\frac{\partial F}{\partial\eta}\right)\right]+sG-\frac{\partial G}{\partial\tau}=0 \quad (15)$$

along with restrictions on the boundary are

$$\begin{cases} F(0,\tau)=0,\ \dfrac{\partial F}{\partial\eta}(0,\tau)=V\dfrac{\partial^2 F}{\partial\eta^2}(0,\tau), G(0,\tau)=0 \\ \dfrac{\partial F}{\partial\eta}(\infty,\tau)\to 0, G(\infty,\tau)\to 0 \end{cases} \quad (16)$$

As mentioned in [16, 19], the stability of the solution is analyzed and hence F($\eta$) = $F_0(\eta)$ and G($\eta$) = $G_0(\eta)$ in equations (14)-(15) to check decay or growth of initial solution of equation (13). For this, linearized eigenvalue problem (17)-(18) has been solved:

$$(1+2\gamma\eta)F_0^{'''}+(2\gamma+f_0)F_0^{''}+f_0^{''}F_0-(2f_0^{'}-s+M)F_0{}'=0 \quad (17)$$

$$(1+2\gamma\eta)G_0^{''}+2\gamma G_0^{'}+\Pr f_0G_0^{'}+\theta_0^{'}F_0-n(f_0^{'}G+\theta_0F_0^{'})+sG=0 \quad (18)$$

along with the restrictions on the boundary are

$$\begin{cases} F_0(0)=0, F_0^{'}(0)=V, G_0(0)=0 \\ F_0^{'}(\infty)=0, G_0(\infty)=0 \end{cases} \quad (19)$$

For flow stability solution $F_0(\eta)$ and $\theta_0(\eta)$, it should be noted that for a fixed entry of $V, Pr, \gamma, M$ and $s$, we determine the smallest $s$, suggested by Harris et al. (2009), we solve the equations (17)-(19).

## IV. RESULT AND DISCUSSION

The boundary value problem consisting of the differential equations (5)-(6) along with boundary restrictions (7) has been computed numerically, using Runge-Kutta Fehlberg method with the shooting technique. Based on the computed results, an analysis of flow and heat transfer has been done for distinct fluid parameters. The results have been presented in terms of figures and tables.

Figure 2 shows the dual nature of the solution exists in flow transportation for $\lambda > 0$ in presence of $V$. The upper branch (depicted by solid line) represents a stable velocity profile. On the other side, the lower branch (depicted by dashed line) represents an unstable velocity profile. Also, the velocity profile shows an asymptotic behavior for both stable and unstable solutions (Figure 2).

**Table 1:** Smallest eigenvalues $s$ at different $\lambda$ when $Pr = 1, \gamma = 0.01, n = 0.5, V = 0.1$ and $M = 0.01$

| $\lambda$ | Upper Solution | Lower Solution |
|---|---|---|
| -0.03 | 0.0063 | -0.0067 |
| 0 | 0.2016 | −0.0940 |
| 0.03 | 0.4160 | −0.1745 |
| 0.04 | 0.4741 | −0.1979 |
| 0.05 | 0.5290 | −0.2177 |
| 0.06 | 0.5821 | −0.2392 |
| 0.08 | 0.6803 | −0.2745 |

Further, the limit of the unstable solution and critical point for $\lambda$ has been found in the presence of slip velocity parameter $V = 0.1$. Figure 3 demonstrates the variation in $f^{''}(0)$ against the outer velocity parameter $\lambda$ in presence of slip velocity. The critical point ($\lambda_c = -0.03211$) and limit of the dual solution is $\lambda_c \le \lambda \le \lambda_r = 0.12651$, when $V = 0.1$, are clearly presented in Figure 3. Table 1 represents the smallest eigenvalue $s$ for stable and unstable solution with distinct entries of outer velocity parameter $\lambda$. The result described in Table 1 explains that $s$ has negative outcomes for unstable solution and positive for stable one. Also, the outcomes of $s$ approaching zero when $\lambda$ approaches to the critical point. Further, the analysis has been done only for the stable solution for distinct fluid parameters.

The plots of velocity profile for various entries of $\gamma$ in presence of slip parameter $V = 0.2$ are shown in Figures 4, 5 and 6 for distinct entries of outer velocity parameter $\lambda = 0, 0.5$ and 2 respectively. Figures 4-5 explain that, in existence of slip velocity, fluid velocity reduces slightly with increasing $\gamma$ up to a certain distance near the stretching surface and then a phase transition occurs, thereafter the fluid velocity curves show trend reversal with increase in $\gamma$. This phase transition in fluid velocity occurs with increasing $\gamma$, near the stretching surface due to the presence of slip velocity. On the other hand, for $\lambda > 1$ (Figure 6), we observed a completely opposite trend but still having a phase transition. Therefore, in all situations of ($\lambda = 0, 0.5, 2$), a transformation of stage occurs in velocity profiles which clearly demonstrates the role of slip effect near the surface.

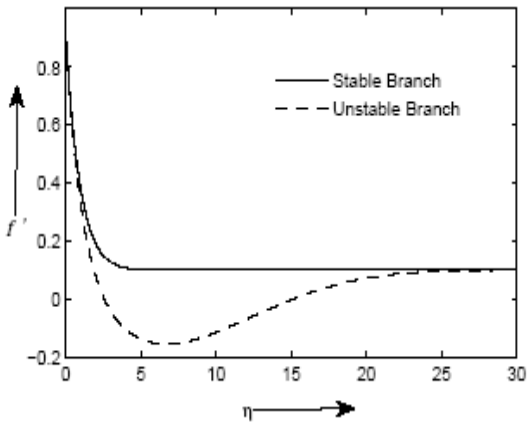


**Figure 2:** $f'(\eta)$ for $\lambda = 0.1$ when $V = 0.1, Pr = 1, \gamma = 0.01, n = 0.5$ and $M = 0.01$

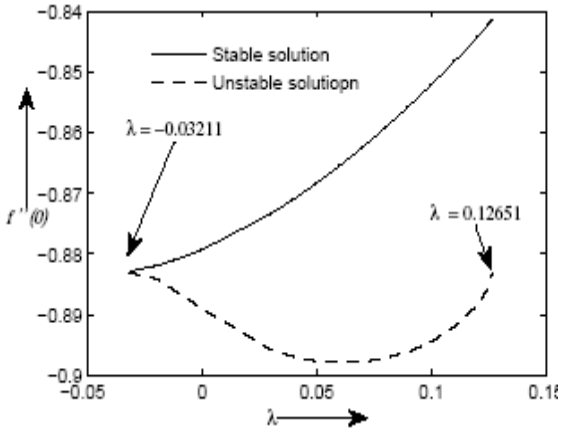


**Figure 3:** Variation in $f''(0)$ for $\lambda = 0.1$ when $V = 0.1, Pr = 1, \gamma = 0.01, n = 0.5$ and $M = 0.01$

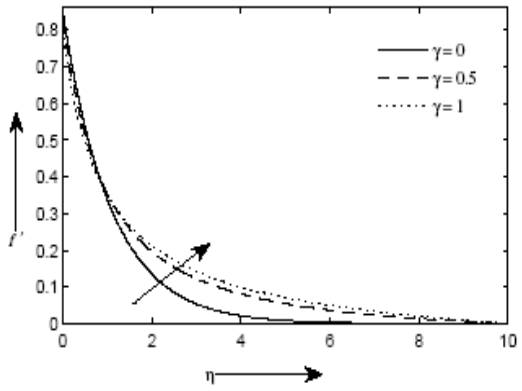


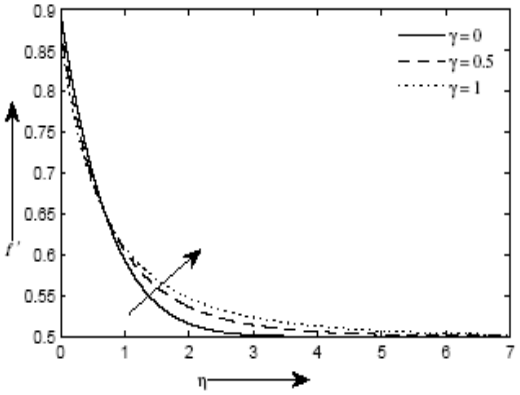


**Figure 4:** $f'(\eta)$ for distinct entries of $\gamma$ with $V = 0.2$, when $\lambda = 0$.
**Figure 5:** $f'(\eta)$ for distinct entries of $\gamma$ with $V = 0.2$, when $\lambda = 0.5$

Figures 7, 8 and 9 show the effects of $\gamma$ (in existence of slip velocity) on the temperature profiles for $\lambda = 0, 0.5$ and 2 respectively. In all situations, the decrease in temperature gradient in noticed. Thus, tem- perature rises with increasing $\gamma$. Further, we noticed that the transition point appears in all the three cases, just as in the velocity profiles (Figures 4-6).

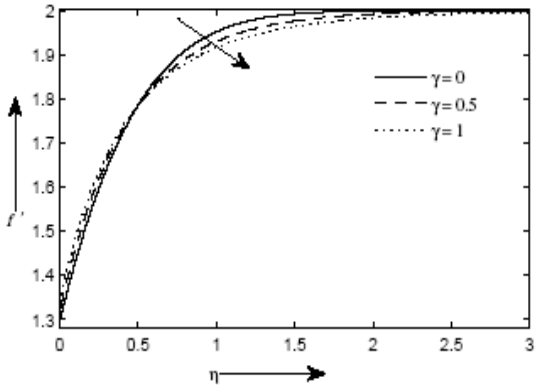


**Figure 6:** $f^{'}(\eta)$ for distinct entries of $\gamma$ with $V = 0.2$, when $\lambda = 2$

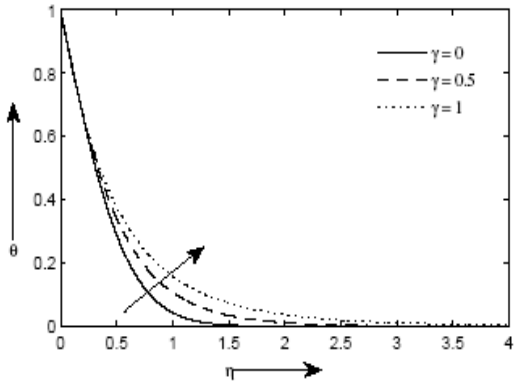


**Figure 7:** $\theta(\eta)$ for distinct entries of $\gamma$ with $V = 0.2$, when $\lambda = 0$

**Table 2:** Computed results of $f^{''}(0)$ and $-\theta'(0)$ for distinct $\gamma$ and $V$ for $Pr = 7, n = 0$ *and* $M = 0$

| | | $V = 0$ | | $V = 0.2$ | |
|---|---|---|---|---|---|
| $\lambda$ | $\gamma$ | $f''(0)$ | $-\theta'(0)$ | $\lambda$ | $\gamma$ |
| 0 | 0 | −1.00001 | 1.89534 | 0 | 0 |
| 0 | 0.5 | −1.18459 | 2.05619 | 0 | 0.5 |
| 0 | 1 | −1.36386 | 2.21193 | 0 | 1 |
| 0.5 | 0 | −0.66726 | 1.98146 | 0.5 | 0 |
| 0.5 | 0.5 | −0.77611 | 2.16816 | 0.5 | 0.5 |
| 0.5 | 1 | −0.87584 | 2.35102 | 0.5 | 1 |
| 2 | 0 | 2.01749 | 2.38607 | 2 | 0 |
| 2 | 0.5 | 2.26076 | 2.61919 | 2 | 0.5 |
| 2 | 1 | 2.48567 | 2.84067 | 2 | 1 |

**Table 2:** gives the computed outcomes of $-\theta^{'}(0)(\propto N_u)$ and $f''(0)(\propto C_f)$ for distinct entries of $\gamma$ and $\lambda$, having slip ($V = 0.2$) and no-slip ($V = 0$) condition. The $f''(0)$ values are negative for $\lambda < 1$, as it exerts a drag on the surface. Also, from Table 2, we noticed that with increasing $V$ , $C_f$ increases and $N_u$ decreases when $\lambda < 1$. Thus friction increases which resulting a decline in velocity when $\lambda < 1$.

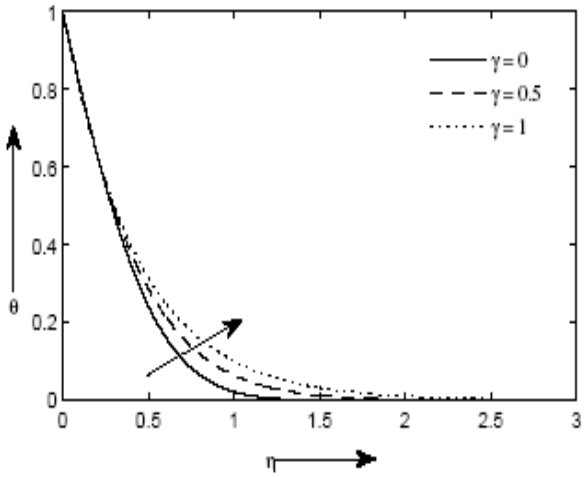


**Figure 8:** θ(η) for distinct entries of γ with V=0.2, when λ = 0.5

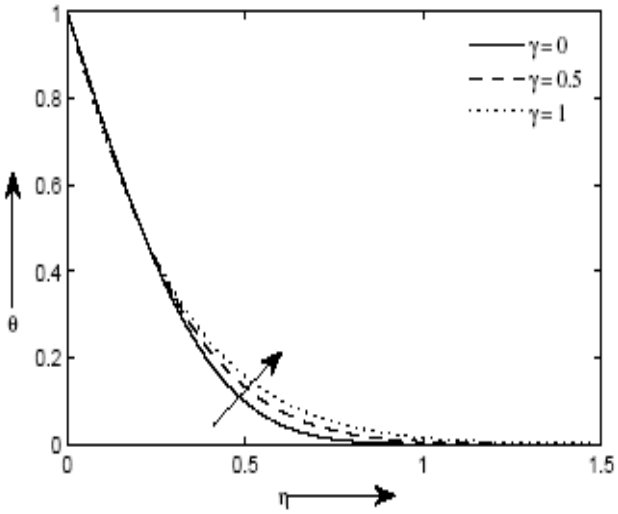


**Figure 9:** θ(η) for distinct entries of γ with V=0.2, when λ = 2

The fluid velocity (Figures 4 and 5) increases for $\lambda < 1$ (after the transition point) because the value of the skin friction reduces with increasing $\gamma$ whereas for $\lambda = 2$, we found a rever- sal trend (Figure 6) due to the opposite variations observed in the $f''(0)$. In addition, we see from Table 2 that $N_u$ raises with increasing $\gamma$ entries for each $\lambda$.

Figures 10, 11 and 12 give the plots of velocity profile for $\lambda = 0, \lambda = 0.5$ and $\lambda = 2$ respectively for distinct entries of magnetic parameter $M$, with slip condition at the surface. The clear separation of curves in each figure demonstrates the significant effect of magnetic field on the fluid flow in existence of partial slip condition. The existence of magnetic field causes a retardation in the fluid velocity (shown by the arrow in Figures 10 and 11) when $\lambda < 1$, while the impact of outer velocity dominates over magnetic impact when $\lambda > 1$, as seen from the opposite trend of velocity for $\lambda > 1$ (Figure 12).

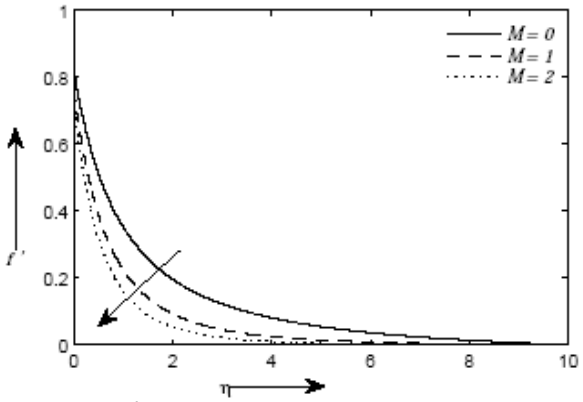


**Figure 10:** $f'(\eta)$ for distinct entries of $M$ with $V = 0.2$, when $\lambda = 0$

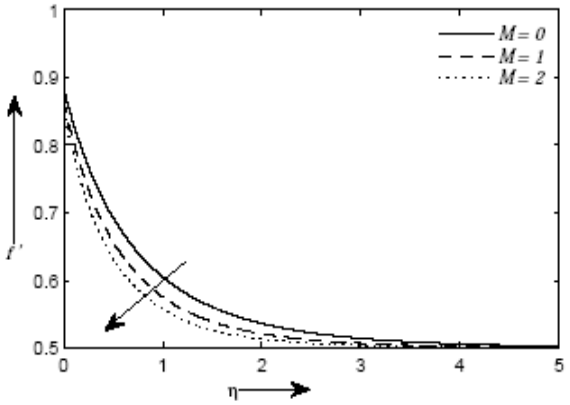


**Figure 11:** $f'(\eta)$ for distinct entries of $M$ with $V = 0.2$, when $\lambda = 0.5$

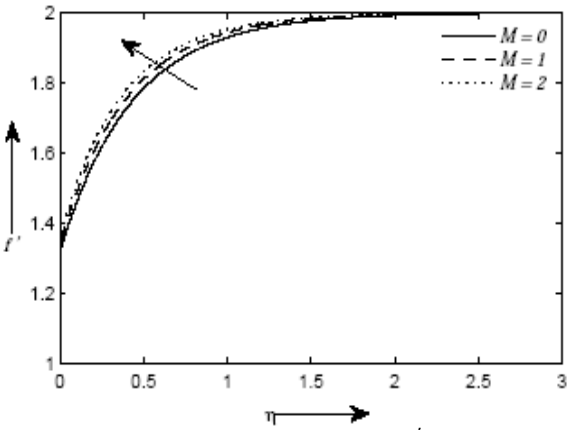


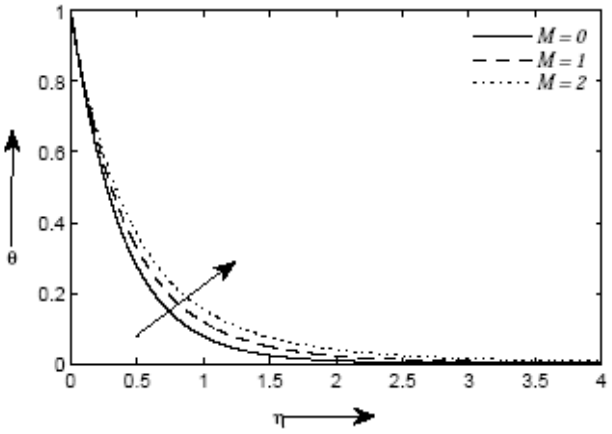


**Figure 12:** $f'(\eta)$ for distinct entries of $M$ with $V = 0.2$, when $\lambda = 2$
**Figure 13:** $\theta(\eta)$ for distinct entries of $M$ with $V = 0.2$, when $\lambda = 0$

**Table 3:** Computed results of $-\theta'(0)$ and $f''(0)$ for distinct entries of $M$ when $\gamma = 0.5, Pr = 7, n = 0.5$ and $V = 0.2$.

| $\lambda$ | $M$ | $-\theta'(0)$ | $f''(0)$ |
|---|---|---|---|
| 0 | 0 | 2.47176 | -0.89621 |
| 0 | 1 | 2.26424 | -1.17917 |
| 0 | 2 | 2.11381 | -1.36415 |
| 0.5 | 0 | 2.68989 | -0.57964 |
| 0.5 | 1 | 2.64240 | -0.67535 |
| 0.5 | 2 | 2.60717 | -0.74758 |
| 2 | 0 | 3.60278 | 1.59258 |
| 2 | 1 | 3.63188 | 1.69564 |
| 2 | 2 | 3.65583 | 1.78417 |

Table 3 gives computed values of $-\theta'(0)$ and $f''(0)$ for distinct entries of $M$.

We notice that as we increase the outer velocity parameter $\lambda$, the variation of magnetic field has a lesser effect on skin friction coefficient. The magnetic field opposes the transport phenomenon because when we increase magnetism, the Lorentz force increases and it offers large interruptions to the transport phenomenon and indirectly leads to rise in the temperature (displayed in Figure 13), as we rise the magnetic intensity. Table 3 gives the computed values of $C_f$ and $N_u$ for distinct entries of $M$ in absence and presence of $\lambda$. For all $\lambda$, as we increase $M$ the magnitude of $C_f$ increases whereas $N_u$ increases for $\lambda > 1$ and decreases for $\lambda < 1$.

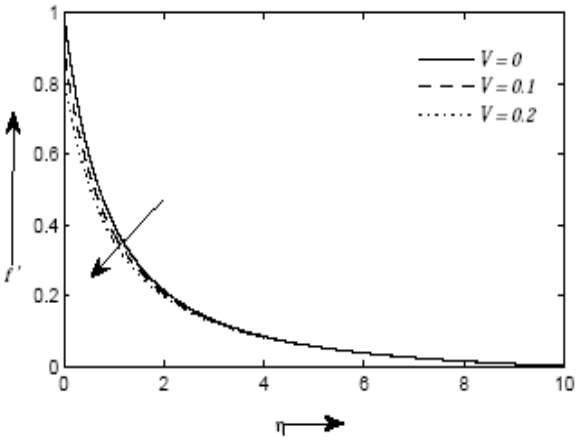


**Figure 14:** $f'(\eta)$ for distinct $V$ when $\lambda = 0$

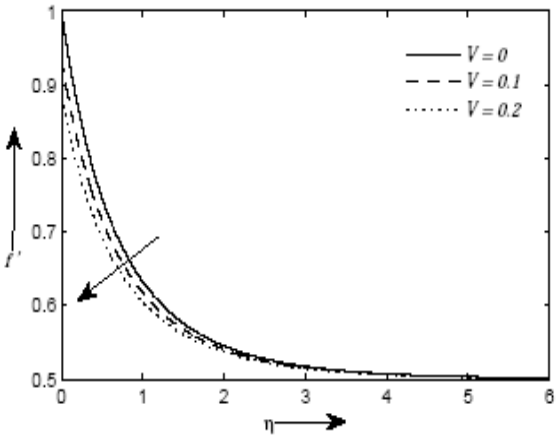


**Figure 15:** $f'(\eta)$ for distinct $V$ when $\lambda = 0.5$

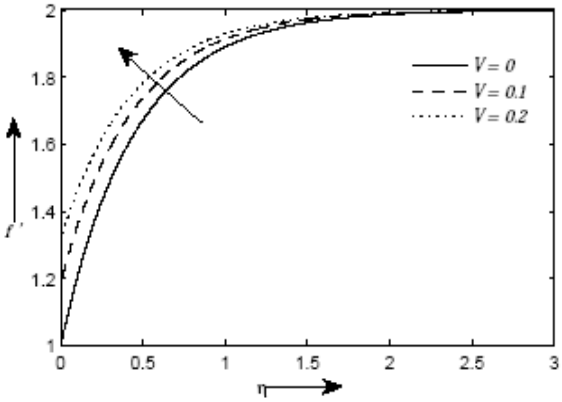


**Figure 16:** $f'(\eta)$ for distinct $V$ when $\lambda = 2$

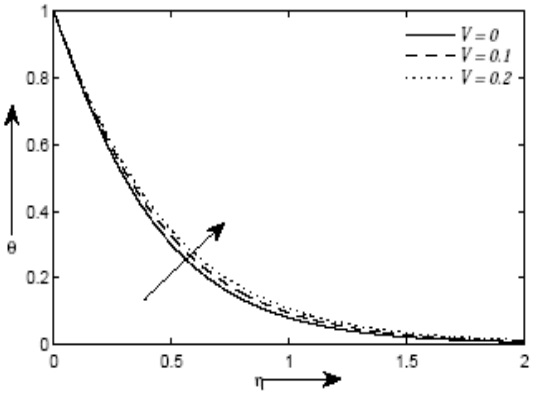


**Figure 17:** $\theta(\eta)$ for distinct $V$ when $\lambda = 0$

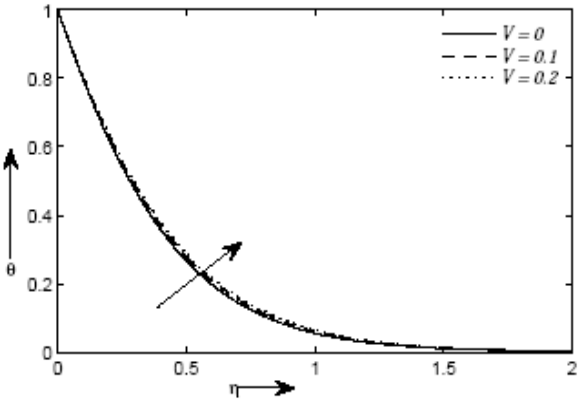


**Figure 18:** $\theta(\eta)$ for distinct $V$ when $\lambda = 0.5$

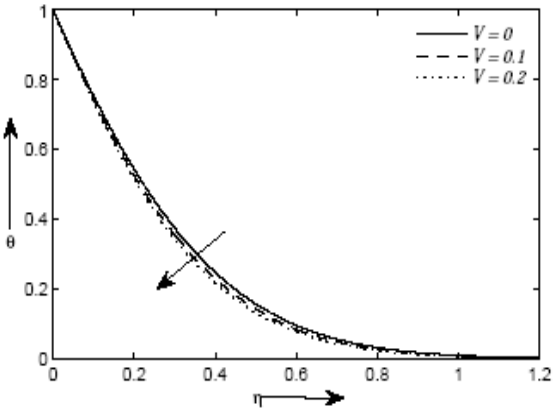


**Figure 19:** $\theta(\eta)$ for distinct $V$ when $\lambda = 2$

Figures 14, 15 and 16 depicted curves of velocity for different entries of $V$ for distinct $\lambda$. We observe that as $V$ increases, there is a reduction (shown by the arrow) in velocity (Figure 14 and 15) for $\lambda < 1$, while a reverse trend is noticed for $\lambda > 1$ (Figure 16). The magnitude of velocity gradient decreases as we move away from the surface and ultimately vanishes.

Figures 17, 18 and 19 represent the temperature curves for different entries of $V$ with different $\lambda$. The rise in temperature is noticed with increasing $V$ when $\lambda < 1$ (Figures 17 and 18), while decline in temperature is

noticed for $\lambda > 1$ (Figure 19). A quick comparison of the velocity curves (Figures 14-16) and the temperature curves (Figures 17-19) showing impact of partial slip indicates that the velocity curves with greater separation are affected more by the partial slip.

# V. CONCLUSION

In this paper, we have formulated and solved numerically the heat and flow transportation problem of an MHD outer velocity flow over a progressively stretching cylinder in horizontal direction with partial slip. The key findings are:

1. Results clearly show the existence of dual nature of the solution. Stable and unstable solution is given by upper and lower branch.
2. The limit of the unstable solution is given as $-0.03211 \leq \lambda \leq 0.12651$ for $V = 0.1$.
3. Slip effect shows a transition point in velocity profiles when we increase the curvature parameter values.
4. Smallest eigenvalue for stable solution is positive and for unstable solution is negative for different outer velocity parameter $\lambda$.

**Conflict of Interests**

The author does not have any conflict of interest regarding the publication of paper.

**Acknowledgement**

The Author expresses his earnest thanks to the reviewers for improvement of the paper.

# References

[1]. Ali, M. E. (1994). Heat transfer characteristics of a continuous stretching surface. *Wrme - und Stoffbertragung*, 29, 227–234.

[2]. Andersson, H. I. (2002). Slip flow past a stretching surface. *Acta Mechanica*, 158, 121–125.

[3]. Ariel, P. (2008). Two dimensional stagnation point flow of an elastico-viscous fluid with partial slip. *ZAMM - Journal of Applied Mathematics and Mechanics / Zeitschrift fr Angewandte Mathematik und Mechanik*, 88, 320–324.

[4]. Awaludin, I. S., Weidman, P. D., & Ishak, A. (2016). Stability analysis of stagnation-point flow over a stretching/shrinking sheet. *AIP Advances*, 6, 045308.

[5]. Crane, L. J. (1970). Flow past a stretching plate. *Zeitschrift fr angewandte Mathematik und Physik*, 21, 645–647.

[6]. Dhanai, R., Rana, P., & Kumar, L. (2015). Multiple solutions of MHD boundary layer flow and heat transfer behavior of nanofluids induced by a power-law stretching/shrinking permeable sheet with viscous dissipation. *Powder Technology*, 273, 62–70.

[7]. Dhanai, R., Rana, P., & Kumar, L. (2016). Critical values in slip flow and heat transfer analysis of non-Newtonian nanofluid utilizing heat source/sink and variable magnetic field: Multiple solutions. *Journal of the Taiwan Institute of Chemical Engineers*, 58, 155–164.

[8]. Gupta, P. S., & Gupta, A. S. (1977). Heat and mass transfer on a stretching sheet with suction or blowing. *The Canadian Journal of Chemical Engineering*, 55, 744–746.

[9]. Harris, S. D., Ingham, D. B., & Pop, I. (2009). Mixed convection boundary layer flow near the stagnation point on a vertical surface in a porous medium: Brinkman model with slip. *Transport Porous Media*, 77, 267–285.

[10]. Ishak, A., Nazar, R., & Pop, I. (2008). Magnetohydrodynamic (MHD) flow and heat transfer due to a stretching cylinder. *Energy Conversion and Management*, 49, 3265–3269.

[11]. Lin, H., & Shih, Y. (1980). Laminar boundary layer heat transfer along static and moving cylinders. *Journal of the Chinese Institute of Engineers*, 3, 73–79.

[12]. Lok, Y. Y., Merkin, J. H., & Pop, I. (2012). Mixed convection flow near the axisymmetric stagnation point on a stretching or shrinking cylinder. *International Journal of Thermal Sciences*, 59, 186–194.

[13]. Mahapatra, T. R., Nandy, S. K., Vajravelu, K., & Van Gorder, R. A. (2012). Stability analysis of the dual solutions for stagnation-point flow over a non-linearly stretching surface. *Meccanica*, 47, 1623–1632.

[14]. Malik, M. Y., Salahuddin, T., Hussain, A., & Bilal, S. (2015). MHD flow of tangent hyperbolic fluid over a stretching cylinder: using Keller box method. *Journal of Magnetism and Magnetic Materials*, 395, 271–276.

[15]. Mat, N. A. A., Arifin, N. M., Nazar, R., & Bachok, N. (2015).Boundary layer stagnation point slip flow and heat transfer towards a shrinking/stretching cylinder over a permeable surface. *Applied Mathematics*, 6, 466–475.

[16]. Merkin, J. H. (1985). On dual solutions occurring in mixed convection in a porous medium. *Journal of Engineering Mathematics*, 20, 171–179.

[17]. Mukhopadhyay, S. (2013). MHD boundary layer slip flow along a stretching cylinder. *Ain Shams Engineering Journal*, 4, 317–324.

[18]. Paullet, J., & Weidman, P. (2007). Analysis of stagnation point flow toward a stretching sheet. *International Journal of Non-Linear Mechanics*, 42, 1084–1091.

[19]. Poply, V., Singh, P., & Yadav, A. K. (2018). Stability analysis of MHD outer velocity flow on a stretching cylinder. *Alexandria Engineering Journal*, 57, 2077–2083.

[20]. Sharma, R., Ishak, A., & Pop, I. (2014). Stability analysis of magnetohydrodynamic stagnation-point flow toward a stretching/shrinking sheet. *Computers and Fluids*, 102, 94–98.

[21]. Singh, P., Tomer, N. S., Kumar, S., & Sinha, D. (2010). MHD oblique stagnation-point flow towards a stretching sheet with heat transfer. *International Journal of Applied Mathematics and Mechanics*, 6(13), 94–111.

[22]. Takhar, H. S., Chamkha, A. J., & Nath, G. (2000). Combined heat and mass transfer along a vertical moving cylinder with a free stream. *Heat and Mass Transfer*, 36, 237–246.

[23]. Vajravelu, K., Prasad, K. V., & Santhi, S. R. (2012). Axisymmetric magneto-hydrodynamic (MHD) flow and heat transfer at a non-isothermal stretching cylinder. *Applied Mathematics and Computation*, 219, 3993–4005.

[24]. Wang, C. Y. (1988). Fluid flow due to a stretching cylinder. *The Physics of Fluids*, 31, 466–468.

[25]. Wang, C. Y., & Ng, C. O. (2011). Slip flow due to a stretching cylinder. *International Journal of Non-Linear Mechanics*, 46, 1191–1194.

[26]. Yadav, R. S., & Sharma, P. R. (2014). "Effects of porous medium on MHD fluid flow along a stretching cylinder," *Annals of Pure and Applied Mathematics*, 6(1), 104–113.